

Dear Axel Lauer (Topical Editor, Geoscientific Model Development),

thank you for your report from 1 March 2017. We have accounted for the comments and suggestions in the revised manuscript version. Please find our replies to the particular comments in the following.

Sincerely

Konrad Deetz and Bernhard Vogel

Referee comments:

My following comments are based on the revised submission by the authors. The authors developed a method of estimating gaseous pollutant emissions from gas flaring for southern West Africa by incorporating various source data and theoretical equations. Gas flaring is not a global issue, but could be considerable at the regional scale, especially in southern West Africa where oil and gas production activities are substantial. I do think this study is very meaningful and innovative, however, the biggest flaw of this study comes from too many assumptions of the input parameters for estimating the emissions.

The key aim of our study is to describe gas flaring emission in southern West Africa (SWA) on a physical basis instead of using emission factors which hides all uncertainties in one number. The number of parameters indicates the complexity of the gas flaring emission. Assumptions are necessary in these cases where measurements were not available.

1) For instance, (1) the authors indicated that “IU14 remarked, that the reaction condition for flaring of $\eta \gg 0.5$ and $\delta > 0.9$ should be the norm in regions”, but why η was set to 0.8 and δ was set to 0.95? The parameters combustion efficiency (η) and availability of combustion air (δ) are strongly dependent on the type of flare and how the flaring process is handled. This can vary significantly from one site to another. For SWA we have no information about these parameters. Therefore we have on the one hand tried to isolate the parameter range according to literature values for general gas flaring (not specifically for SWA) and on the other hand conducted a sensitivity study to estimate the uncertainty (see Fig. 8a,b in the manuscript).

Regarding the combustion efficiency η the studies IU14, Strosher (2000) and EPA (1985) were used. Based on these studies we have decided for $\eta = 0.8$. Regarding δ we have decided for $\delta = 0.95$ by following the remark of IU14 $\delta \geq 0.9$ and by assuming that the flaring conditions are not perfect in SWA and therefore that there is a deficiency in combustion air $\delta < 1.0$. Based on these limits we have decided for $\delta = 0.95$. We agree that the parameter selection of η and δ was not motivated detailed enough. Therefore we have updated the relevant passage accordingly:

“The combustion efficiency η and the availability of combustion air δ significantly depend on the flaring characteristics (e.g. available technique to steer the flaring process and how the staff takes care of the flaring procedure), which can vary significantly from one side to another. For SWA no information about these parameters is available. The parameter range at least was isolated according to literature values for gas flaring in general (not specifically for SWA). IU14 remarked, that the reaction condition for flaring of $\eta \gg 0.5$ and $\delta \geq 0.9$ should be the norm in regions, where the effective utilization of this gas is not available or not economically. Strosher (2000) indicates a combustion efficiency of solution gas at oil-field battery sites between 0.62 and 0.82, and 0.96 for

flaring of natural gas in the open atmosphere under turbulent conditions. EPA (1985) shows combustion efficiencies between 0.982 and 1 for measurements on a flare screening facility. Based on these information the combustion efficiency η was set to 0.8. Regarding the availability of combustion air we on the one hand follow IU14 with $\delta \geq 0.9$ and on the other hand assume that the flaring conditions are not perfect in SWA, which means that there is a deficiency in combustion air $\delta < 1.0$. Therefore $\delta = 0.9$ was used for this study.”

2) The specific heat capacity of associated petroleum gas should be highly dependent on its chemical composition. The application of a constant value is not appropriate.

The specific heat capacity c_p (equation (2) in the manuscript) is that for the exhaust gas and not for the fuel gas. We agree that c_p depends on the chemical composition of the fuel gas and that c_p is spatiotemporally not constant. Since we use a spatiotemporal constant chemical composition of the fuel gas (based on Sonibare and Akeredolu (2004)) it is consistent also to use a constant c_p value.

There is no information of c_p of the fuel gas of the flares in SWA. Often waste gases from oil refineries are burned which can have other chemical compositions as the natural gas of this site has. Therefore even with a known chemical composition of the natural gas, the uncertainty in c_p will stay.

Table 1 shows c_p values for

I - used for this study, according to VDI 3782 (1985),

II-X - single components of the exhaust gas,

XI - the mixture of gases (II-X) according to the exhaust gas composition which was calculated from IU14 combustion equations.

Tab. 1 – Comparison of the specific heat capacity c_p for several gases.

	c_p (J kg ⁻¹ K ⁻¹)	Flow rate F (m ³ s ⁻¹) relative to this study ($F \sim 1/c_p$)
(I) This study*	1070.366	1
(II) Carbon dioxide	846	-
(III) Carbon monoxide	1040	-
(IV) Water	1870	-
(V) Hydrogen	14400	-
(VI) Oxygen	912	-
(VII) Nitrogen	1040	-
(VIII) Sulfur dioxide	632	-
(IX) Nitrous monoxide	1000.9	-
(X) Nitrous dioxide	632	-
(XI) Mixture of gases** ($C_{p,mix} = \sum \frac{n_i}{n} c_{p,i}$)	1110	0.965

*VDI 3782 (1985) using fuel gas density ρ_f

** flare mean of TP15

We have calculated (XI) for every flare of TP15 and the variation is below 2 J kg⁻¹ K⁻¹. When comparing (I) and (XI), the uncertainty when using (I) instead of (XI) is below 5%. Compared to the other sources of uncertainty (e.g. IU14 parameters, gauge pressure) this is negligible. We have added a comment in the manuscript:

“The value is consistent with the derived mean specific heat capacity for TP15 with an uncertainty below 5%.”

3) The estimation of fuel gas density highly depends on the gauge pressure. It is indicated by the author the gauge pressure varied from 0 – 34kPa. By taking 0 and 34kPa as inputs, respectively, the range of estimated fuel gas densities could be 3 – 4 times different. However, the authors didn't explain why 34kPa was taken.

The gauge pressure is as uncertain as the selection of η and δ . As indicated in the manuscript, Bader et al. (2011) pointed out that the low-pressure single point flares, as the most common flare type for onshore facilities, operate at pressures below 10 psi (pressure above ambient pressure).

API (2007) remarks that most subsonic-flare seal drums operate in the range from 0-5 psi (pressure above ambient pressure). Therefore we have decided to use 5psi, the mean value between the limits 0 and 10 psi. The uncertainty due to the gauge pressure is shown in Fig. 8b for (0, 5 and 10 psi) and linked with that the influence on the fuel gas density. The uncertainty owing to the gauge pressure is part of the overall uncertainty estimation: (+20/-25 %).

4) Although the authors spent lengthy discussions in uncertainty analysis of different input parameters, the results of this study are not informative. As part of the field campaign DACCIWA, the mission should at least investigate some region-specific parameters of the fuel gas such as gauge pressure.

The assessment of the uncertainty the authors see as a key aspect of the study on hand. Without this analysis the study would be incomplete or would pretend certainty and robustness where the current level of knowledge has low confidence.

The DACCIWA field campaign took place from 1 June 2016 to 31 July 2016. This campaign includes (a) the three ground-based so called supersites Savé (Benin), Kumasi (Ghana) and Ile-Ife (Nigeria), which were measuring from 13 June to 31 July 2016, (b) radiosondes and (c) aircraft measurements from the three aircrafts: DLR Falcon, SAFIRE ATR-42 and the British Antarctic Survey (BAS) Twin Otter.

Regarding (a): Savé measured meteorological parameters and in addition the concentrations of ozone, nitrous monoxide, nitrous dioxide, carbon monoxide and isoprene as well as biogenic fluxes. Kumasi and Ile-Ife measured only meteorological parameters.

Regarding (c): The three research aircrafts conducted in total 50 missions (155 flight hours). This includes the three EUFAR (European Facility for Airborne Research) missions OLACTA (Observing the Low-level Atmospheric Circulation in Tropical Atlantic, 10 flight hours), MICWA (Mid-level Inversions and Cloudiness in SWA, 10 flight hours) and APSOWA (Atmosphere Pollution from Shipping and Oil platforms in West Africa, 10 flight hours).

The following objectives were targeted for the aircrafts: characterization of stratus clouds and their interaction with aerosol; quantification of city emissions from Lomé, Accra, Abidjan, Cotonou and Kumasi; characterization of power plant emissions, oil and gas flaring; air pollution from shipping; effects of clouds and radiation; interaction between the land-sea breeze and clouds; measurement of BVOCs and the examination of dust and biomass burning aerosol.

The aircrafts measured meteorological parameters, trace gas and aerosol concentrations as well as cloud droplet and aerosol size distributions and the aerosol composition.

Based on this short overview of the DACCIWA field campaign, the following remarks have to be made according to the referee comment (4):

- The air pollution from flaring was not a key aspect of DACCIWA. It is just one of the sources of air pollution which contributes to the atmospheric composition of SWA.
- The supersites do not contribute to the analysis of the flaring emissions.

- The aircrafts were not allowed to enter the Nigerian airspace and therefore the extended onshore and offshore oil fields in the Niger Delta have not been observed (see Fig. 1 below). This means the only flares reachable in SWA were the sporadic offshore flares south of Ivory Coast and Ghana (see Fig. 2 below).
- Out of the 50 aircraft missions only 2 were explicitly dedicated to flaring.
- Aircraft observation can provide the concentration of trace gases and aerosols from a source but they neither can provide information about the emissions nor about flare specific information like gauge pressure or specific heat capacity.
- To get information about the characteristics of the flare stack, the flaring process and the composition of the fuel gas, a detailed and long-term study directly at the flaring sites would have been necessary. We cannot expect that the gauge pressure is spatiotemporally constant. It is very likely that it significantly varies between several sites and during different working processes at the flaring site. These observations (long-term or short-term) could neither be handled within DACCIWA nor would be granted by the authorities or the oil companies. The oil companies do not cooperate in providing these parameters since flaring is a controversial topic in society and politics.
- The EUFAR mission APSOWA aims to characterize gaseous and particulate pollutants emitted by shipping and oil and gas extraction platforms off the coast of West Africa. These observations shows flare related peaks in sulfur dioxide (~8 ppb), carbon dioxide (~175 ppb) and nitrous dioxide (~7 ppb). However, aircraft observations are not constructive in deriving the parameters needed for the parameterization which is presented in this study, even if a sufficient number of flights (statistics in terms of different flares and number of observations) would have been dedicated to analyze the flaring.
- The very sporadic measurements of flaring concentrations are also not appropriate for direct evaluation of the output of the flaring parameterization because the emissions have to be transformed to concentrations. Therefore a link of an atmospheric dispersion model with the emission parameterization is necessary to be comparable with the aircraft observations. This brings further uncertainty into the intercomparison, especially if only a very small number of aircraft detections of flaring pollution are available. We have added a passage in section 5 to denote this problem:

“Gas flaring is just one of the sources of air pollution in SWA and therefore the DACCIWA field campaign in June-July flaring cannot solely focus on flaring. To provide detailed measurements of the flaring characteristics would go beyond the scope of DACCIWA. However, within the DACCIWA aircraft campaign, the EUFAR (European Facility for Airborne Research) mission APSOWA (Atmosphere Pollution from Shipping and Oil platforms in West Africa) was conducted to characterize gaseous and particulate pollutants emitted by shipping and oil and gas extraction platforms off the coast of West Africa. The authors hope that the results of APSOWA bring further insight in the characteristics of gas flaring in SWA.”

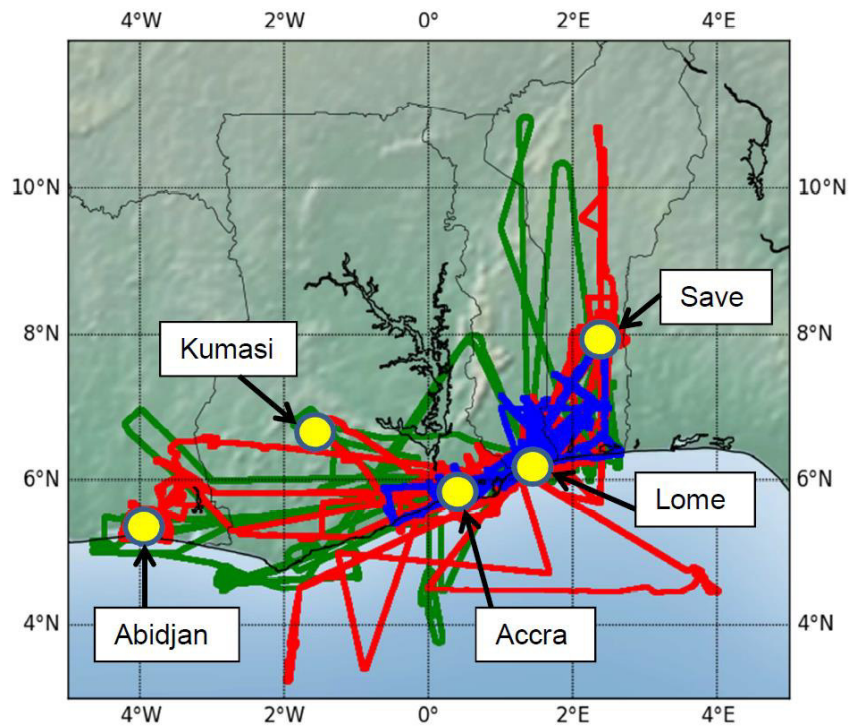


Fig. 1. – Overview of flights conducted by the three research aircraft during the DACCIWA field campaign. The DLR Falcon is denoted in green, the SAFIRE ATR-42 in red and the BAS Twin Otter in blue. Nigeria (east of Benin) shows no aircraft observations. (This figure is not part of the manuscript.)

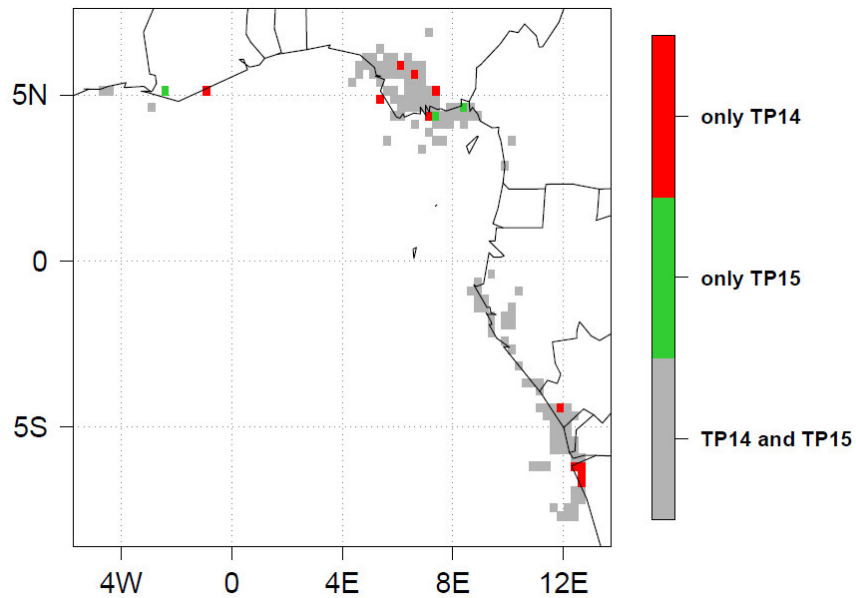


Fig. 2. – Location of gas flaring in June-July 2014 (red), June-July 2015 (green) and both periods (grey). The countries in the north are Ivory Coast, Ghana, Togo, Benin and Nigeria (from west to east). (This figure is also part of the manuscript (Fig. 1).)

5) Most importantly, the emissions should be evaluated by the model as the campaign should have a suite of measurement data. Without this validation, this manuscript seems not coincide with scope of GMD. Therefore, I suggest a resubmission by comprehensively evaluating the emissions created in this study.

This refers to the referee comment (4). DACCIWA has not provided data which allows a comprehensive evaluation. In the manuscript we therefore have conducted a detailed evaluation against existing flaring emission inventories. The aim of our study was to shed light on flaring as a side topic of DACCIWA, including all the uncertainties which are linked to the description of gas flaring emission. When starting with this study, very low information was available for the flaring in that region. Within our study we bring the information together which are available (e.g. the gas composition of Sonibare and Akeredolu (2004) and the space-borne observations of VNP (flare location and flare activity) to describe the flaring emissions on a physical basis using IU14. This can be seen as a significant step forward in comparison to the description via emission factors. We do not deny the uncertainties within the parameterization; on the contrary we disassemble the uncertainties to lay them open, instead of hiding them in the description of emission factors.

To further raise the knowledge about the characteristics and the amount of gas flaring in that region, the will of the local politicians together with the cooperation of the oil producing industry is necessary.

We have described our method in detail, evaluated it against existing inventories and made the source code free available for the reader/user in terms of reproducibility. Within the aims and scope of GMD our study is located in “development and technical papers, describing developments such as new parameterizations of technical aspects of running models such as the reproducibility of results”.

1 Development of a new gas flaring emission data set for southern West Africa

2
3 Konrad Deetz, Bernhard Vogel

4
5 Karlsruhe Institute of Technology (KIT), Institute of Meteorology and Climate Research – Troposphere Research
6 (IMK-TRO), Hermann-von-Helmholtz 1, 76344 Eggenstein-Leopoldshafen

7 8 HIGHLIGHTS

- 9
10 - Development of a new gas flaring emission parameterization for air pollution modeling.
11 - Combination of remote sensing observation and physical based combustion calculation.
12 - Application to the significant gas flaring region southern West Africa.
13 - Comprehensive assessing of the parameterization uncertainties.
14 - Comparison with existing gas flaring emission inventories.
15

16 Keywords:

17
18 Gas flaring
19 Emission parameterization
20 Emission uncertainty
21 Pollution modeling
22 Carbon dioxide
23

24 ABSTRACT

25
26 A new gas flaring emission parameterization has been developed which combines remote sensing
27 observations using VIIRS nighttime data with combustion equations. The parameterization has been
28 applied to southern West Africa, including the Niger Delta as a region which is highly exposed to gas
29 flaring. Two two-month datasets for June-July 2014 and 2015 were created. The parameterization
30 delivers emissions of CO, CO₂, NO and NO₂. A flaring climatology for both time periods has been
31 derived. The uncertainties owing to cloud cover, parameter selection, natural gas composition and
32 the interannual differences are assessed. Largest uncertainties in the emission estimation are linked
33 to the parameter selection. It can be shown that the flaring emissions in Nigeria have significantly
34 decreased by 25% from 2014 to 2015. Existing emission inventories were used for validation. CO₂
35 emissions with the estimated uncertainty in brackets of 2.7 (^{3.6}/_{0.5}) Tg y⁻¹ for 2014 and 2.0 (^{2.7}/_{0.4}) Tg
36 y⁻¹ for 2015 were derived. Regarding the uncertainty range, the emission estimate is in the same
37 order of magnitude compared to existing emission inventories with a tendency for underestimation.
38 The deviations might be attributed to a shortage in information about the combustion efficiency
39 within southern West Africa, the decreasing trend in gas flaring or inconsistent emission sector
40 definitions. The parameterization source code is available as a package of R scripts.
41

42 1. Introduction

43
44 Gas flaring is a globally used method to dispose flammable, toxic or corrosive vapors to less reactive
45 compounds at oil production sites and refineries. In regions of insufficient transportation
46 infrastructure or missing consumers, flaring is also commonly applied.
47 CDIAC (2015a) estimated the global gas flaring emission of carbon dioxide to 267.7 million tons
48 (0.83% of total emissions) in 2008. Flaring and venting of gas significantly contributes to the

49 greenhouse gas emissions and therefore to the global climate change. The five countries with the
50 highest flaring amount in billion cubic meters (bcm) are Russia (35), Nigeria (15), Iran (10), Iraq (10)
51 and USA (5) (World Bank, 2012). These estimates were produced by National Oceanic and
52 Atmospheric Administration (NOAA) using Defense Meteorological Satellite Program (DMSP) remote
53 sensing data. Preliminary updates in global flaring estimates from NOAA for 2013 and 2014 are
54 available at http://ngdc.noaa.gov/eog/viirs/download_global_flare.html.

55 In recent time, especially with the development of remote sensing observation techniques (e.g.
56 Elvidge et al. (1997, 2013)), emissions from gas flaring moved in the focus of atmospheric research
57 involving the efforts in reducing the pollution and the waste of resources. The World Bank led the
58 initiatives “Global Gas Flaring Reduction Partnership” (GGFR) and “Zero Routine Flaring by 2030” to
59 promote the efficient use of flare gas.

60 Instead of relying on national statistics of gas production and consumption for estimating the flaring
61 amount, remote sensing techniques can estimate the flaring amount directly via multispectral data
62 (Elvidge et al., 2013). Elvidge et al. (2009) developed a 15 year dataset of global and national gas
63 flaring efficiency from 1994 to 2008 by using data from DMSP. Elvidge et al. (2015) presented
64 methods to derive global surveys of natural gas flaring using DMSP. For 2012 they have identified
65 7467 flares globally, with an estimated volume of flared gas of 143 (± 13.6) bcm. Doumbia et al.
66 (2014) combined DMSP with emission factors for flaring, to estimate the flaring emissions for SWA.
67 The satellite product Visible Infrared Imaging Radiometer Suite (VIIRS) Nightfire (Elvidge et al., 2013),
68 which is free available as “VIIRS Nightfire Nighttime Detection and Characterization of Combustion
69 Sources” (VIIRS, 2015a) (VNF hereafter), is now the most widely used product to derive flaring
70 emissions from satellite imagery. By using VNF, Zhang et al. (2015) estimated the methane
71 consumption and the release of CO₂ from gas flaring for the northern U.S. which agree with field data
72 within an uncertainty range of $\pm 50\%$.

73 Also in the second largest flaring country Nigeria, the awareness of gas flaring increases. Nigeria
74 shows the fourth highest number of flare sites (approx. 300) worldwide after USA, Russia and Canada
75 (Elvidge et al., 2015). On gasflaretracker.ng the attention of the government, industry and society is
76 called to the flaring problem by interactive maps of flare infrastructure, amounts and costs. The
77 implications of gas flaring in Nigeria are far-reaching. It influences the environment by noise and
78 deterioration of the air quality (Osuji and Avwiri, 2005). Nwankwo and Ogagarue (2011) have
79 measured higher concentrations of heavy metals in surface water of a gas flared environment in
80 Delta State Nigeria. Adverse ecological and bacterial spectrum modifications by gas flaring are
81 indicated by Nwaugo et al. (2006). Gas flaring also causes acid rain which causes economic burden
82 via rapid corrosion of zinc roofs (Ekpoh and Obia, 2010) and causes retardation in crop growth owing
83 to high temperatures (Dung et al., 2008).

84 The project DACCIWA (Dynamics-aerosol-chemistry-cloud interactions in West Africa, Knippertz et al.
85 (2015)) investigates the influence of anthropogenic and natural emissions on the atmospheric
86 composition over SWA, including the flaring hotspot Nigeria, to quantify the effects on meteorology
87 and cloud characteristics. To consider the SWA gas flaring emissions (e.g. in an atmospheric model),
88 this study presents a method to derive emission fluxes by combining the state of the art flaring
89 detection VNF and the combustion equations of Ismail and Umukoro (2014) which does not use
90 emission factors. The new parameterization is robust and easy to apply to new research questions
91 according flexibility in the spatiotemporal resolution.

92 The parameterization is presented in Section 2. Results of the application to SWA, including the
93 spatial distribution of gas flaring, the emission estimation and the uncertainty assessment are

94 investigated in Section 3. Section 4 places the emission estimates in the context of existing
95 inventories. The results are summarized and discussed in Section 5.

96

97 **2. Parameterization of gas flaring emissions**

98

99 The new parameterization for gas flaring presented here, is based on VIIRS Nightfire Nighttime
100 Detection and Characterization of Combustion Sources (VNF hereafter) and the combustion
101 equations of Ismail and Umukoro (2014) (IU14 hereafter).

102

103 **2.1 Remote sensing identification of gas flares**

104

105 VIIRS (Visible Infrared Imaging Radiometer Suite) is a scanning radiometer for visible and infrared
106 light on board the sun-synchronous Suomi National Polar-orbiting Partnership weather satellite
107 (Suomi-NPP) (NASA, 2016). It can detect combustion sources at night (e.g. bush fires or gas flares) by
108 spectral band M10. To confirm these sources and to eliminate noise, the Day/Night Band (DNB), M7,
109 M8 and M12 are used in addition. By fitting these measured spectra to the Planck radiation curve,
110 background and source temperatures can be deduced (VIIRS, 2015a).

111 The data is freely available as daily cloud corrected data from March 2014 to present. The files
112 include among others the location of the combustion sources, source temperature T_s , radiant heat H
113 and time of observation. VNF does not distinguish between the different combustion sources (e.g.
114 wild fires or flaring). To extract the flaring information from VNF a postprocessing is necessary. For
115 this study we have decided for a two month period of observation. This allows a compilation of a
116 flaring climatology in terms of the locations and emissions and a robust estimation of uncertainty
117 owing to cloud coverage and parameters that have to be prescribed for IU14. We have selected the
118 month June and July because the gas flaring emission dataset will be used within the regional online-
119 coupled chemistry model COSMO-ART (Vogel et al., 2009) during the measurement campaign of the
120 project DACCIWA, which took place in June/July 2016. This campaign includes airborne, ground
121 based and remote sensing observations of meteorological conditions and air pollution
122 characteristics. COSMO-ART is one of the forecasting models of the DACCIWA campaign and delivers
123 spatiotemporal aerosol/chemistry distributions. The data for June/July 2014 and June/July 2015 are
124 used to allow also for an interannual comparison and to assess the uncertainty owing to changes in
125 flare processes (e.g. built-up or dismantling, increase or decrease in combustion). The dataset
126 includes the countries which can affect SWA with their flaring emissions, in particular Ivory Coast,
127 Ghana, Nigeria, Cameroon, Gabon, Congo, the Democratic Republic of the Congo and Angola. The
128 extraction of the flaring information from the VNF data (VNF_{flare} hereafter) was realized by the Earth
129 Observation Group of NOAA. Within VNF_{flare} a csv file for every SWA flare is available, containing the
130 flaring history in June/July 2014 and 2015. For this study we use the location, source temperature
131 and radiant heat.

132

133 **2.2 Emission estimation method**

134

135 The principle emission estimation methodology used in this study follows IU14. The gas flaring
136 emissions are estimated based on combustion equations for incomplete combustion including six
137 flaring conditions given in Tab. 1. The equations are introduced in detail in IU14 and are therefore
138 not presented here. This section concentrates on the application of the method of IU14 to the
139 VNF_{flare} data and the research domain SWA.

140

141 **Tab.1.** Reaction types for incomplete combustion of flared gas, depending on availability of sulfur in the flared gas and the
 142 temperature in the combustion zone which determines the formation of NO and NO₂.
 143

Reaction type	Sulfur in flared gas	Source temperature (K)	NO _x formation
1	No	< 1200	no
2	Yes	< 1200	no
3	No	$1200 \leq T_s \leq 1600$	only NO
4	Yes	$1200 \leq T_s \leq 1600$	only NO
5	No	> 1600	NO and NO ₂
6	Yes	> 1600	NO and NO ₂

144
 145 As input, IU14 needs the natural gas composition C of the fuel input of the flare, the source
 146 temperature T_s (temperature in the combustion zone), and the flare characteristics including
 147 combustion efficiency η (1 is complete combustion without Carbon monoxide formation) and
 148 availability of combustion air δ (above 1 means excess and below 1 means deficiency). In addition
 149 we need the flow rate F , the gauge pressure of the fuel gas in the flare p_g , and the fraction of total
 150 reaction energy that is radiated f . The value for f is estimated by averaging a table of literature
 151 values for f given in Guigard et al. (2000). The IU14 input is summarized in Tab. 2.
 152

153 **Tab.2.** Variables and parameters needed for IU14 or for deriving the fluxes of the air pollutants
 154

Parameter	Description	Reference	Unit
C	Natural gas composition	Sonibare and Akeredolu (2004)	%
T_s	Source temperature	VNF _{flare} (VIIRS, 2015a)	K
η	Combustion efficiency	0.8 (IU14)	-
δ	Availability of combustion air	0.95 (IU14)	-
H	Radiant heat	VNF _{flare} (VIIRS, 2015a)	MW
F	Flow rate	VNF _{flare} (VIIRS, 2015a), (VDI 3782, 1985)	m ³ s ⁻¹
p_g	Gauge pressure	34.475 (API, 2007)	kPa
f	Fraction of radiated heat	0.27 (Guigard et al., 2000)	-

155
 156 The natural gas composition is taken from Sonibare and Akeredolu (2004). They have measured the
 157 molar composition of Nigerian natural gas in the Niger Delta area for ten gas flow stations. For this
 158 study we have calculated the average over these stations and merged the data according their
 159 number of carbon atoms (Tab. 3). H₂S fraction is rather low because it was detected only in two out
 160 of the ten flow stations.
 161

162 **Tab.3.** Molar composition of natural gas in Niger Delta (Nigeria) based on the measurements of Sonibare and Akeredolu
 163 (2004), averaged over ten flow station. The hydrocarbons are merged according to the number of C atoms.
 164

Constituent	Fraction (%)
Methane (CH ₄)	78.47
Ethane (C ₂ H ₆)	6.16
Propane (C ₃ H ₈)	5.50
Butane (C ₄ H ₁₀)	5.19
Pentane (C ₅ H ₁₂)	3.95
Hexane (C ₆ H ₁₄)	0.36
Carbon dioxide (CO ₂)	0.305
Nitrogen (N ₂)	0.06
Hydrogen sulfide (H ₂ S)	0.005

166 The source Temperature T_S is taken from VNF_{flare} . The combustion efficiency η and the availability of
 167 combustion air δ significantly depend on the flaring characteristics (e.g. available technique to steer
 168 the flaring process and how the staff takes care of the flaring procedure), which can vary significantly
 169 from one side to another. For SWA no information about these parameters is available. The
 170 parameter range at least was isolated according to literature values for gas flaring in general (not
 171 specifically for SWA). IU14 remarked, that the reaction condition for flaring of $\eta \gg 0.5$ and $\delta \geq 0.9$
 172 should be the norm in regions, where the effective utilization of this gas is not available or not
 173 economically. Strosher (2000) indicates a combustion efficiency of solution gas at oil-field battery
 174 sites between 0.62 and 0.82, and 0.96 for flaring of natural gas in the open atmosphere under
 175 turbulent conditions. EPA (1985) shows combustion efficiencies between 0.982 and 1 for
 176 measurements on a flare screening facility. Based on these information ~~the~~ combustion efficiency η
 177 was set to 0.8. Regarding the availability of combustion air we on the one hand follow IU14 with
 178 $\delta \geq 0.9$ and on the other hand assume that the flaring conditions are not perfect in SWA, which
 179 means that there is a deficiency in combustion air $\delta < 1.0$. Therefore $\delta = 0.9$ was used for this
 180 study. -Section 3.3.2 will shed light on the uncertainty which arises from η and δ via a parameter
 181 sensitivity study. The authors strongly recommend a careful selection of η and δ since unrealistic
 182 combinations (e.g. higher combustion efficiencies with rather low availability of combustion air) can
 183 lead to negative NO and NO₂ emissions.

184 The flow rate, gauge pressure and fraction of radiated heat are not included in the parameterization
 185 of IU14 but are necessary to derive the mass emission rates which can be used as emission data for
 186 an atmospheric dispersion model.

187 The flow rate F ($\text{m}^3 \text{s}^{-1}$) is derived from Eq. 1 (VDI 3782, 1985)

$$188 \quad F = M / (c_p (T_S - T_A)), \quad (1)$$

189 where M is the heat flow in MW, c_p the mean specific heat capacity of the emissions, T_S the source
 190 temperature and T_A the ambient temperature. VDI 3782 (1985) provides a value of the mean specific
 191 heat capacity of
 192

$$193 \quad c_p = 1.36 \cdot 10^{-3} \text{ MW s m}^{-3} \text{ K}^{-1} \quad (2)$$

194 which is derived for a pit coal firing but VDI 3782 (1985) denotes, that this can be used for other flue
 195 gases as well since potential deviations are negligible. The value is consistent with the derived mean
 196 specific heat capacity for TP15 with an uncertainty below 5%. For the ambient temperature T_A we
 197 use 298.15K as a fixed value, representative for the tropical region. Within a sensitivity study
 198 regarding the influence of T_A on the heat flow, we have used the averaged heat flow and source
 199 temperature of all flares within the time period June/July 2015 and varied the ambient temperature
 200 between 293K and 303K, as a reasonable temperature range in the tropical regions. The resulting
 201 maximum difference in the heat flow is 0.0036 m³ s⁻¹. Therefore we assume that the uncertainties
 202 using a fixed climatological value for the ambient temperature are negligible. For the application of
 203 this inventory to other regions the ambient temperature might be adapted. By using Eq. 1 and 2 the
 204 heat flow F can be derived as
 205

$$206 \quad F = M / (1.36 \cdot 10^{-3} (T_S - 298.15)), \quad (3)$$

207 with T_S in K.

208 We assume that the emitted heat flow M is equal to the total reaction energy of the flare. VNF_{flare}
 209 only detects the energy fraction that is radiated H and not the total energy M . By using the radiant
 210

211 heat H (observed by VNF_{flare}) and the factor f (fraction of H to the total reaction energy, Guigard et
 212 al., 2000), we estimate M as $H \cdot 1/f$. For the source temperature T_S we use the VNF_{flare} observations.
 213 The estimation of the fuel gas density, which is necessary to transform the flow rate F into an
 214 emission, is problematic due to the lack of data concerning the technical setup of the SWA flares. We
 215 assume that the dominating flare type is a low-pressure single point flare. Bader et al. (2011) pointed
 216 out that these flares are the most common flare type for onshore facilities that operate at low
 217 pressure (below 10 psi (69 kPa) above ambient pressure) and API (2007) remarks that most subsonic-
 218 flare seal drums operate in the range from 0 psi to 5 psi (34 kPa). Therefore we have decided for a
 219 gauge pressure p_g of 5 psi (34 kPa) above ambient pressure. Via Eq. 3 we can calculate the fuel gas
 220 density ρ_f

$$\rho_f = p_f / (R / (M_f T_A)), \quad (3)$$

221
 222 where p_f is the fuel gas pressure as the sum of ambient pressure (10.1325 kPa, taken as const) and
 223 gauge pressure p_g . R is the universal gas constant, M_f the molar mass of the fuel gas and T_A the
 224 ambient temperature (298.15 K, taken as const). Finally, the emission E (kg s^{-1}) of a species i is given
 225 by
 226
 227
 228

$$E_i = \frac{m_i}{m_{\text{total}}} \rho_f F, \quad (4)$$

229
 230 where m_i is the mass of the species i and m_{total} the total mass of the fuel gas, both delivered by the
 231 parameterization of IU14.

232 The combustion calculations within IU14 provide the species water, hydrogen, oxygen, nitrogen,
 233 carbon monoxide, carbon dioxide, sulfur dioxide, nitrogen oxide and nitrogen dioxide. In the
 234 following only the latter five are considered. However, no black carbon or volatile organic
 235 compounds (VOCs) are considered by IU14, although they are not negligible. Johnson et al. (2011)
 236 estimated the mean black carbon emission for a large-scale flare at a gas plant in Uzbekistan to be
 237 7400 g h^{-1} and Strosher (1996) measured the concentration of predominant VOCs 5 m above the gas
 238 flare in Alberta with 458.6 mg m^{-3} . However, owing to the missing representation of black carbon and
 239 VOCs in IU14, these compounds are not considered in this study.

240 By using the source code written in R (R Core Team, 2013) delivered by this study, the user can define
 241 the grid size independently (e.g. model grid) on which the flaring point sources are allocated.

242

243 3. Results

244

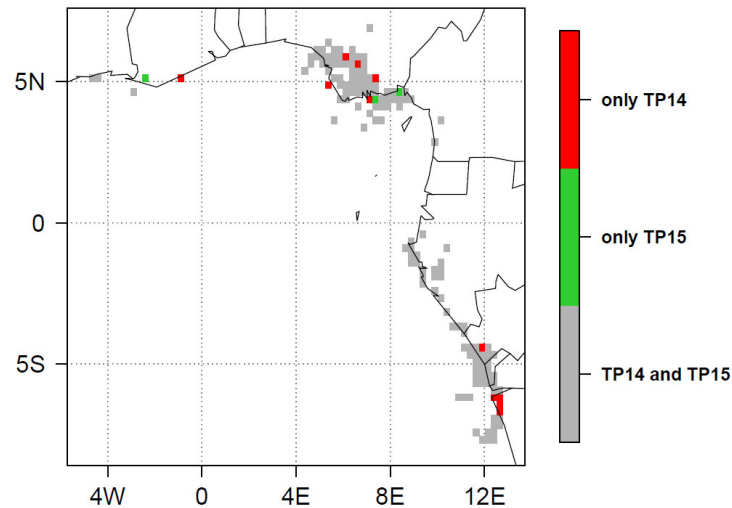
245 3.1 Spatial distribution of gas flaring in SWA

246

247 We have selected the two time periods June/July 2014 (TP14) and June/July 2015 (TP15) of VNF_{flare}
 248 over SWA (61 observations respectively).

249 In the preparation of this work we have compared the locations of the flares of TP14 with the Google
 250 Earth imagery (Google Earth, 2014) (not shown). Only the onshore flares are visible in Google Earth.
 251 This visual verification reveals that 72% of the VNF_{flare} detected onshore flares are visible in Google
 252 Earth. It is very likely that the hit rate is much higher since it is often the case that the Google Earth
 253 image quality is not good enough for verification or the images are not up to date. This comparison
 254 indicates that VNF_{flare} is an effective method to identify the flares in SWA.

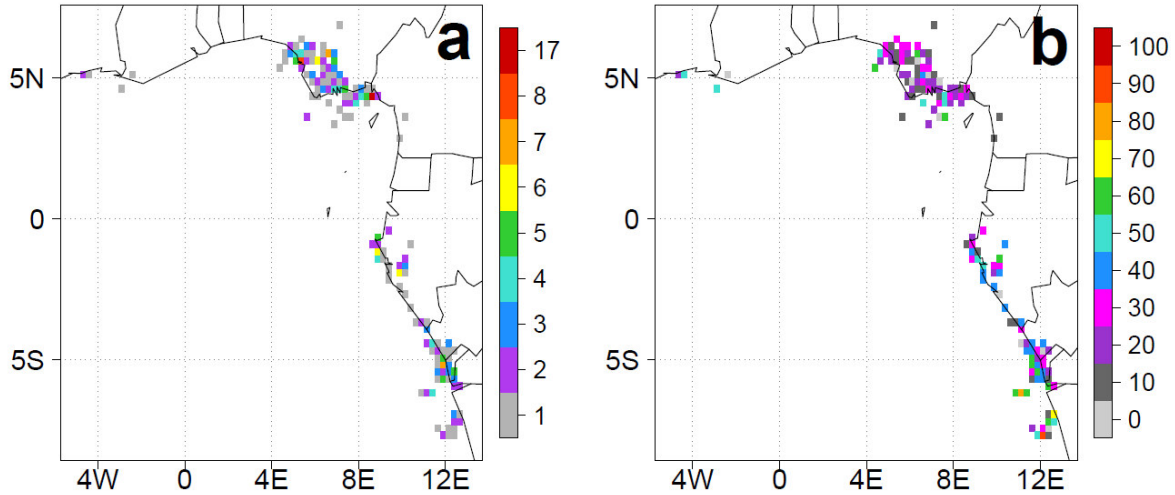
255 For the following analysis we have allocated the flares to a grid with a mesh size of 0.25° (28 km)
 256 from 8°S to 7°N and from 5°W to 13°E and calculated the emissions for both time periods. A grid box
 257 with flaring is denoted as flare box hereafter. Fig. 1 emphasizes the areas in which $\text{VNF}_{\text{flare}}$ detects
 258 flares only in TP14 (TP15) in red (green) color and in grey the areas with flaring in both periods.
 259
 260



261
 262 **Fig.1.** Flaring area for TP14 and TP15. Red (green) boxes denote areas with flaring only for TP14 (TP15). For the grey areas,
 263 flaring is detected in both time periods.
 264
 265

266 Remarkable are the dominating flaring areas in the Niger Delta and the adjacent offshore regions in
 267 the Gulf of Guinea. Also in the coastal region of Gabon, Congo, Angola and sporadically in Ghana and
 268 offshore of Ivory Coast, flaring occurs. By comparing TP14 and TP15 more red than green areas are
 269 visible, especially in southern Nigeria, which indicates a reduction in the flaring area from 2014 to
 270 2015. The red areas contribute 12% to the total CO_2 emissions of TP14. $\text{VNF}_{\text{flare}}$ detects 335 flares in
 271 2014 and 312 flares in 2015 which means a reduction of about 7% (counted are those which deliver
 272 at least once a value for T_s and H in the time period). 61% of that reduction is related to Nigeria. A
 273 decrease in CO_2 from 1994 to 2010, particularly in the onshore platforms is indicated by Doumbia et
 274 al. (2014).

275 Fig. 2 shows the density of flares (a) and the flaring activity (b) per flare box for TP15. The results are
 276 similar to TP14, therefore only the TP15 is displayed here.
 277



278
279

280 **Fig.2.** (a) Number of flares per flare box and (b) flaring activity (%) per flare box within TP15. A flaring activity of 100%
281 means that every day on the 61 day period in June/July flaring was detected.

282

283 The highest flare density can be found offshore in the border area of Nigeria and Cameroon with 17
284 flares per flare box. The offshore flaring density is smaller than onshore (Fig. 2a) whereas the highest
285 flaring activity can be found offshore (Fig. 2b). This could be linked to the increased masking of flares
286 by clouds over land. The large onshore flaring area of the Niger Delta shows a comparable low flaring
287 activity of 10-30%. Highest values can be found offshore of the Democratic Republic of the Congo
288 and Angola of 50-90%. How the interannual variability of flaring reflects in the amount of flaring
289 emissions is analyzed in section 3.3.4.

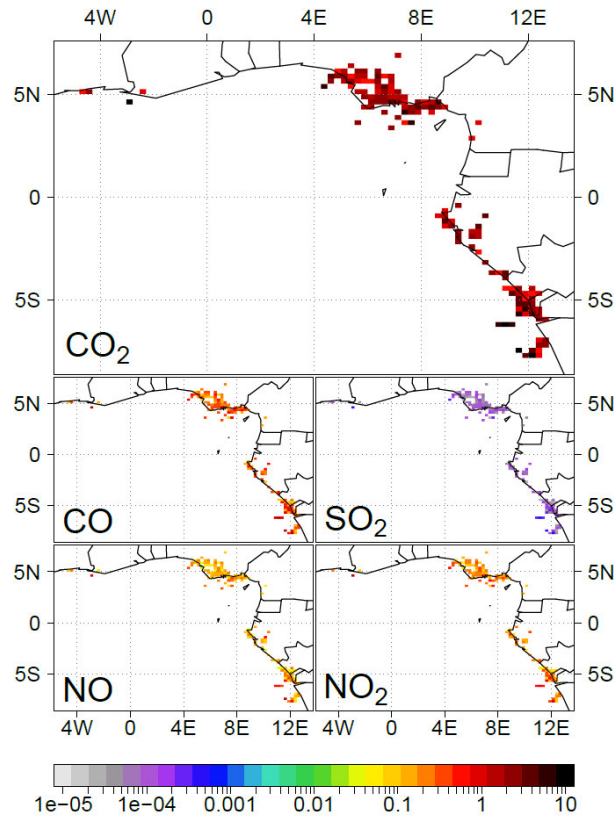
290

291 3.2 Emission estimation

292

293 For the emission estimation we have used a climatological approach (E_{clim}). For every flare the
294 temporal averages of source temperature and radiant heat over TP14 and TP15 were used to
295 calculate the emissions. Therefore in this approach all flares, detected in the time period, are active
296 at once with their mean emission strength. This method has the advantage that most likely all flares
297 in the domain are captured even if a fraction of them is covered by clouds at certain days. However,
298 this could lead to an emission overestimation because not all available flares are active at once. This
299 problem of separating between flares which are not active and flares which are active but covered by
300 clouds and therefore not visible for VNF_{flare} is picked up again in Section 3.3.1. Fig. 3 shows the
301 emissions of CO_2 , CO , SO_2 , NO and NO_2 in t h^{-1} for TP15.

302



303
304
305
306
307

Fig.3. Flaring emissions for TP15 within E_{clim} in t h^{-1} considering CO_2 , CO, SO_2 , NO and NO_2 . For better visibility the emissions are displayed as colored grid boxes although the emissions are still point sources and not area sources.

308 Highest emissions are derived for carbon dioxide, followed by carbon monoxide, nitrogen dioxide
309 and nitrogen oxide. Sulfur dioxide shows lowest emissions since these emissions do not depend on
310 combustion processes but only on the natural gas composition (see Tab. 3) and the amount of flared
311 gas (IU14). Due to the use of the averaged measurements of Sonibare and Akeredolu (2004), local
312 variations of hydrogen sulfide concentrations in the natural gas cannot be taken into account.
313 Hydrogen sulfide is the only source of sulfur in the flared gas and therefore determines the emission
314 of sulfur dioxide. To assess this uncertainty, a sensitivity study with different hydrogen sulfide
315 concentrations is given in Section 3.3.5.

316

317 3.3 Estimation of uncertainties

318

319 In the following section the most relevant uncertainties are presented together with approaches for
320 their assessment. This includes the uncertainty concerning the flare detection in the presence of
321 cloud cover, the uncertainty in the determination of the emitted heat flow H via the fraction of
322 radiated heat f , the uncertainty in the choice of the IU14 parameters and the changes in flare
323 operation from one year to another as well as the influence of the spatial variability of hydrogen
324 sulfide in the natural gas on the sulfur dioxide emissions. Apart from Section 3.3.4 all uncertainty
325 estimations are confined to TP15.

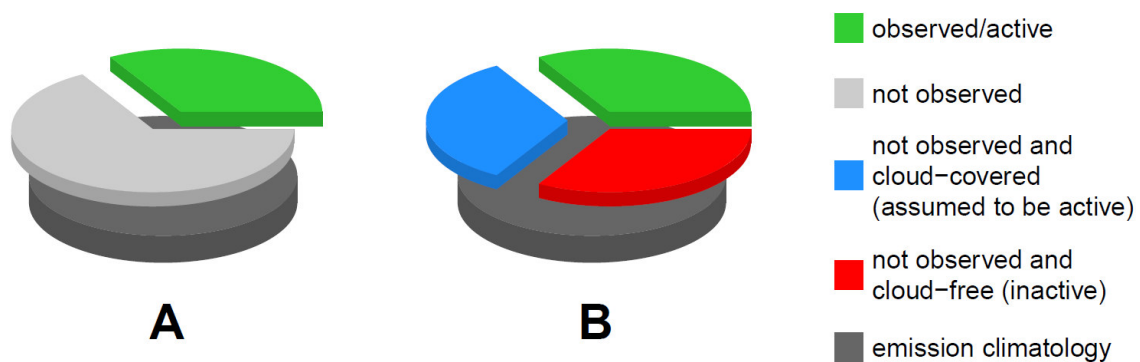
326

327 3.3.1 Uncertainty due to cloud cover

328

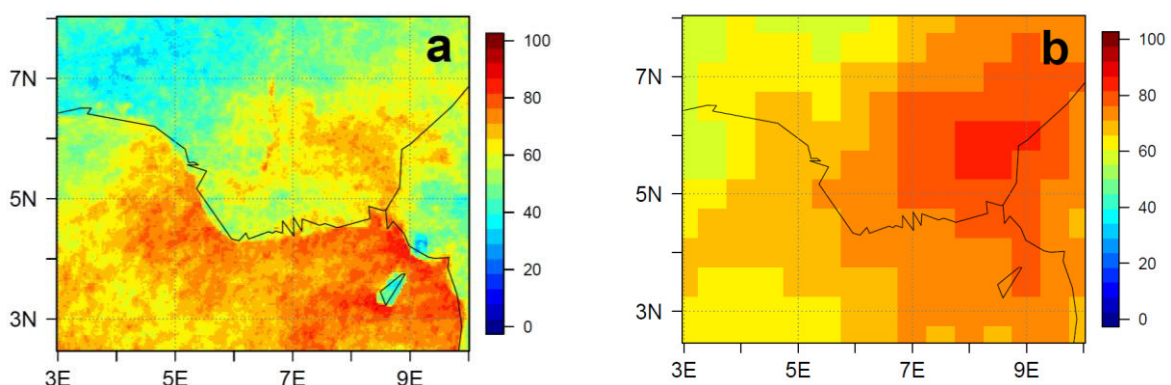
329 In this section we want to estimate the emission error due to cloud-covered flares and present a
330 method to derive daily emissions by considering the contribution of these masked flares. In Section

331 3.2 a climatological data set of flaring emissions (E_{clim}) was derived, in which all available flares are
 332 active with their mean emission strength. This dataset therefore does not include a day to day
 333 variation. If an emission dataset with a daily variability is required, the problem arises that usually
 334 parts of the scene observed by the satellite are covered by clouds and therefore the emissions are
 335 likely underestimated. VNF_{flare} includes the locations of all flares independent whether there are
 336 active or not. This entity is illustrated by the closed dark grey pie in Fig. 4A and 4B. By comparing the
 337 flares which are observed/active at a certain day and the total number of flares, a separation
 338 between observed (green pie in Fig. 4A) and not observed (light grey pie in Fig. 4A) is possible. In
 339 addition VNF_{flare} delivers a cloud mask for all of the flare detections. Therefore it is possible to
 340 separate the light grey pie of the not observed flares in (a) cloud-free and inactive (light blue pie in
 341 Fig. 4B) and (b) cloud-covered and unknown flaring status (blue pie in Fig. 4B).
 342 To estimate the error due to active but cloud-covered flares, we assume that all of these flares are
 343 active with their mean emission strength observed in June/July 2015.
 344



345
 346 **Fig.4.** Pie charts illustrating the flaring emission uncertainty assessment due to cloud cover for TP15. The entity of the flares
 347 within the emission climatology (E_{clim}) is given as closed grey pie in the bottom of **A** and **B**. **A** distinguishes between flares
 348 which are detected/active at a certain day (green) and the complement of undetected flares (light grey). In **B** the light grey
 349 slice of **A** is separated in a cloud-covered (blue) and cloud-free (red) part by using the cloud mask of VNF_{flare} . Flares which
 350 are not detected by VNF_{flare} and covered by clouds are taken as active. Flares which are not detected by VNF_{flare} and are not
 351 covered by clouds are taken as inactive.
 352

353
 354 Fig. 5 illustrates the mean cloud cover exemplarily for the greater Niger Delta area using (a)
 355 instantaneous cloud fractional cover (CFC) from the geostationary Meteosat Second Generation 3
 356 (MSG3) (CM SAF, 2015, copyright (2015) EUMETSAT) for every day of TP15 around the time of VNF
 357 observation (Suomi-NPP overflight approx. at 1 UTC) and (b) the sun-synchronous Aqua/AIRS
 358 (Mirador, 2016).
 359

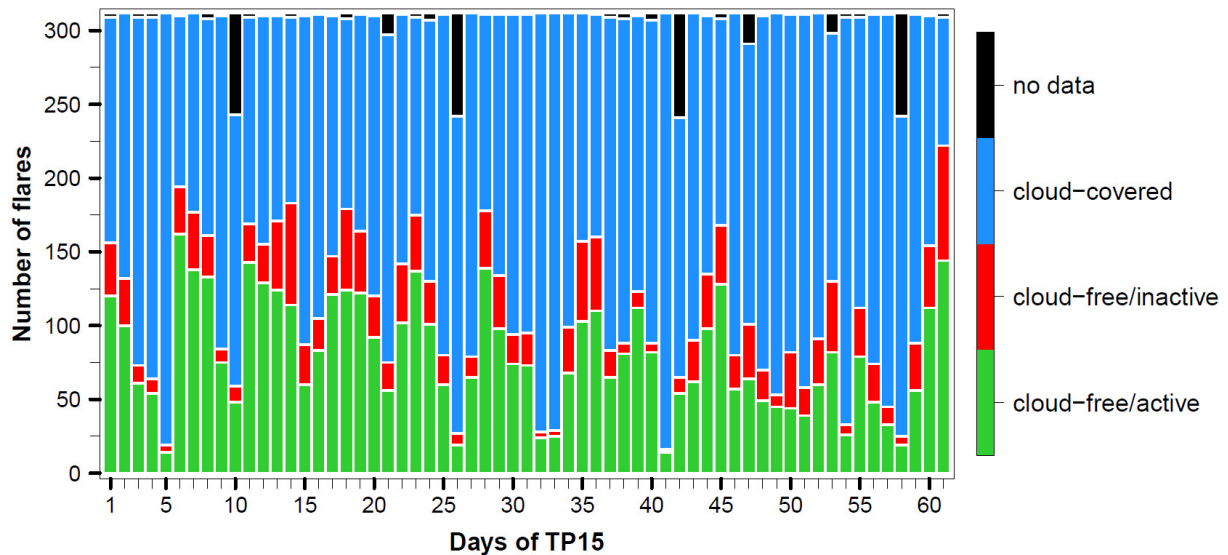


361 **Fig.5.** Fractional cloud cover (%) observed from (a) the geostationary MSG3 and (b) the sun-synchronous Aqua/AIRS,
 362 averaged over TP15 around the time of VNF observation (approx. 1 UTC).
 363

364 Fig. 5a shows that the onshore flaring area for TP15 is in mean covered with clouds by 50-70%. For
 365 the offshore flaring area it is even higher with 70-90%. Therefore it is very likely that flares are
 366 frequently masked by clouds and therefore not detected by VNF. However, we suspect that the
 367 MSG3 cloud product underestimates (overestimates) the onshore (offshore) cloud cover when
 368 comparing with the findings of van der Linden et al. (2015). The high offshore coverage and the
 369 distinct land-water separation might be caused by overestimating low clouds in the presence of a
 370 warm and moist tropical ocean.

371 Fig. 5b shows a cloud climatology using Aqua/AIRS Nighttime data (Mirador, 2016). The Aqua/AIRS
 372 climatology shows higher cloud cover over land and no distinct separation between water and land
 373 surface. Both products identify the highest onshore cloud cover in the northeast of Port Harcourt
 374 (4.8°N, 7.0°E) and have similar values in the Nigerian offshore region (containing the offshore flares)
 375 of about 70-80%. The major difference in the climatologies appears onshore between 4.5°N and 6°N.
 376 This area includes the majority of the Nigerian onshore flares. This reveals a relatively high
 377 uncertainty in the estimation of nocturnal low cloud coverage from remote sensing.

378 Fig. 6 shows the number of flares per day in TP15, separated in the categories: cloud-free/active
 379 (green), cloud-free/inactive (red) and cloud-covered (blue). Flares with no or incomplete data are
 380 coded in black. E_{clim} includes 312 flares which are at least once active in TP15. On average only 26% of
 381 the total flaring area is active at once, 9% is verifiable inactive and 63% is cloud-covered. By taking
 382 into account only the cloud-free information instead of the climatological approach of E_{clim} , on
 383 average 63% of the flares are not considered at a certain day. By assuming that all of these cloud-
 384 covered flares are active, a remarkable underestimation can be expected.

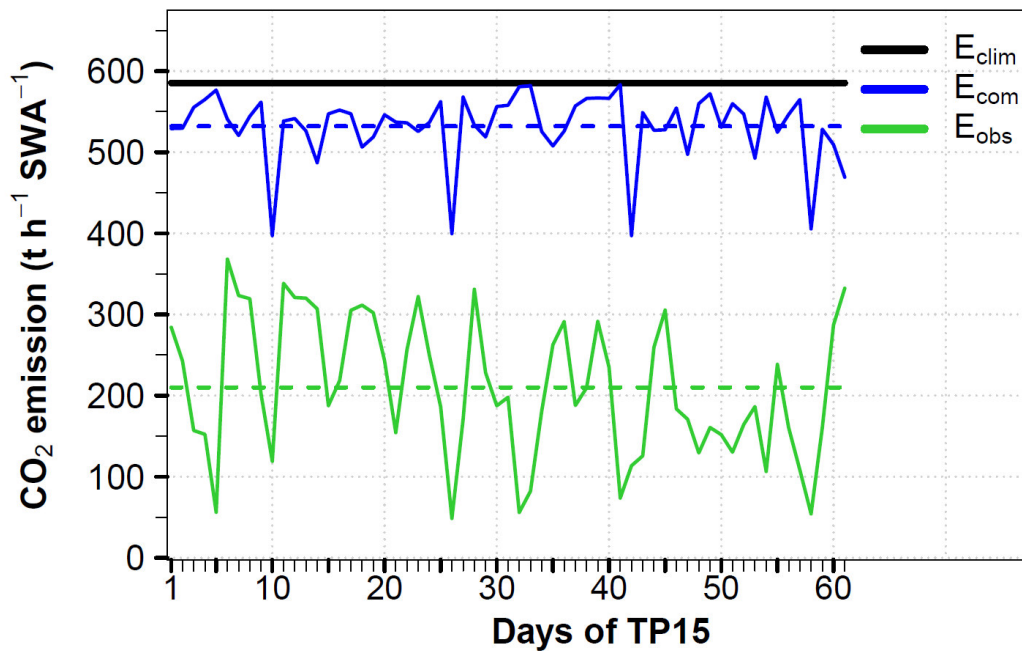


385 **Fig.6.** Number of flares per day in TP15 which are cloud-free and active (green), cloud-free and inactive (red) and cloud-
 386 covered (blue). Flares with no or incomplete data are denoted in black. The color coding follows Fig. 4B. Considered are the
 387 312 flares which deliver at least once a value for T_s and H in TP15.
 388
 389
 390

391 In addition to E_{clim} two further emission inventories are introduced: E_{obs} only considers the actual
 392 daily observed flares (linked to the green flares in Fig. 6). To consider also the contribution of active
 393 but cloud-covered flares, E_{com} combines the green and the blue flares of Fig. 6.

394 To allow for consistency, all three inventories use the emissions derived from the flare specific
 395 temporal averages of the source temperature and the radiant heat over TP14 and TP15 respectively.

396 We avoid calculating the emissions from instantaneous source temperatures because this is linked to
 397 high uncertainty depending on the atmospheric conditions (Mikhail Zhizhin, personal
 398 communication). The temporal averages allow for robustness. Therefore the three inventories only
 399 differ in the selection of the active flares per day but not in the underlying emissions. E_{clim} uses all
 400 flares at a certain day, E_{obs} considers only the flares which are cloud-free and active and E_{com}
 401 considers E_{obs} plus the cloud-covered flares, by assuming that all of the cloud-covered flares are
 402 active. Nevertheless we have included a further inventory in Tab. 5 which uses instantaneous source
 403 temperature and radiant for the emission derivation (E_{clim} , instant. input) to assess the differences
 404 towards the averaged input. Fig. 7 shows the total CO₂ emissions of the SWA area from E_{clim} in black,
 405 from E_{obs} in green and from E_{com} in blue.
 406



407
 408 **Fig.7.** Daily CO₂ emission estimations (t h⁻¹) within TP15 from flaring, summed up over the SWA area as denoted in Fig. 1 for
 409 the three emission inventories: E_{clim} (climatology, black solid line), E_{obs} (daily VNF_{flare} observations, green solid line and
 410 temporal average as green dashed line) and E_{com} (sum of daily VNF_{flare} observations and emissions from cloud-covered
 411 flares, blue solid line and temporal average as blue dashed line). The periodical drop of the blue line is linked to reduced
 412 data coverage (compare with black bars in Fig. 6).
 413
 414

415 The dashed lines denote the temporal averages of E_{obs} and E_{com} . On average E_{com} is only 9% smaller
 416 than E_{clim} which is assumed to be in the range of uncertainty. Therefore both inventories are
 417 equitable in this study. The user can decide whether a temporal resolved or a climatological
 418 approach fits best to their research question.

419 The emissions of E_{obs} are strongly reduced (64%) compared to E_{clim} as expected. The use of E_{obs} would
 420 significantly underestimate the emissions and is therefore not appropriate for an application. Since
 421 E_{obs} does not take into account cloud-covered flares at all and E_{com} in contrast sees all cloud-covered
 422 flares as active, the difference between these inventories can be used to assess the uncertainty
 423 arising from flares masked by clouds. Fig. 7 shows a mean difference between E_{obs} and E_{com} of about
 424 61%. Therefore while using E_{obs} as a flaring emission inventory in an application, an underestimation
 425 of the emissions of 61% has to be considered.

426 These emission estimations contain different information. E_{clim} includes all flares of the domain
 427 invariant but can overestimate the emissions. E_{obs} shows the VNF_{flare} reality, including a temporal

428 development, but cannot consider the cloud-covered flares. E_{com} combines the climatological
 429 information of E_{clim} for flares which are not observable at a certain time and the temporal resolution
 430 of VNF_{flare} in E_{obs} . However this approach is based on the assumption that all cloud-covered flares are
 431 active, which can be seen as an estimation upwards. Therefore the most likely amount of emissions is
 432 expected between E_{obs} and E_{com} .

433

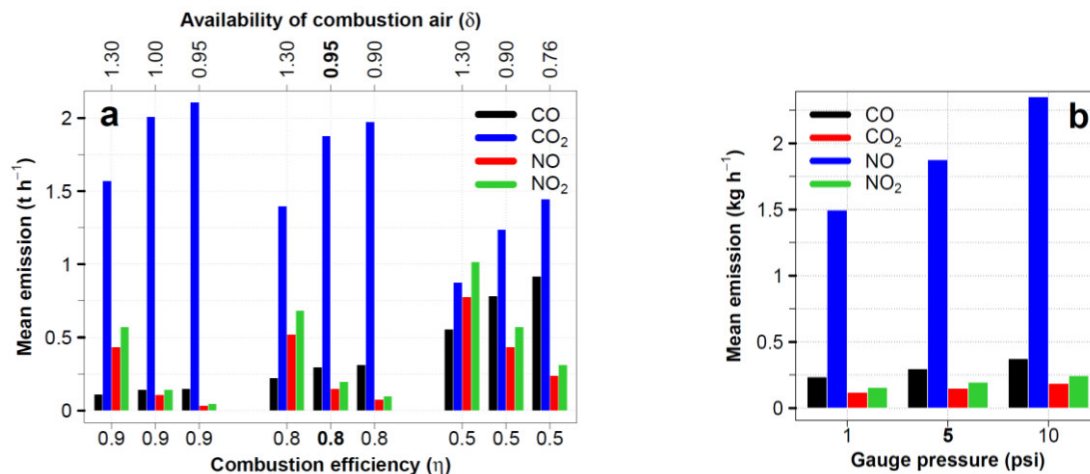
434 3.3.2 Uncertainty due to IU14 input parameters

435

436 To assess the uncertainty which arises from the combustion efficiency η and the availability of
 437 combustion air δ , a sensitivity study has been carried out. The exact values for the SWA flares are
 438 unknown and very likely highly variable from one flare to another, depending on the flare type and
 439 operation. Fig. 8a shows the flaring emissions averaged over SWA and TP15 for CO, CO₂, NO and NO₂.
 440 The parameters η and δ are varied referring to IU14. A complete combustion ($\eta = 1$) does not
 441 produce CO emissions since all carbon is transformed to CO₂ (not shown). With decreasing η and δ ,
 442 the CO and CO₂ emissions increase. Concerning CO we assume the lower limit for $\eta = 0.9$ and
 443 $\delta = 1.3$ (left of Fig. 8a) and the upper limit for $\eta = 0.5$ and $\delta = 0.76$ (right of Fig. 8a). The values
 444 used for this study are located in the center of Fig. 8a (printed in bold). By taking the latter as
 445 reference, the lower (upper) limit leads to a decrease (increase) in CO emission of -63% (+208%). For
 446 CO₂ we derived an lower (upper) limit of -53% (+12%).

447 A higher availability of combustion air allows an enhanced formation of NO and NO₂. Therefore NO_x
 448 emissions increase with decreasing η . In contrast these emissions decrease with an increase in the
 449 combustion efficiency (δ). The higher the efficiency the more oxygen is forming CO₂ instead of NO_x.
 450 We assume the lower limit for $\eta = 0.9$ and $\delta = 0.95$ and the upper limit for $\eta = 0.5$ and $\delta = 1.30$.
 451 Taking again the central parameter set of Fig. 8a as reference, the lower (upper) limit leads to a
 452 decrease (increase) in NO emission of -76% (+420%).

453



454 **Fig.8.** Flaring emissions ($t h^{-1}$) spatiotemporally averaged over SWA and TP15 depending on (a) combustion efficiency η and
 455 availability of combustion air δ for a gauge pressure of 5 psi and (b) gauge pressure (psi) for $\eta = 0.8$ and $\delta = 0.95$. SO₂ is
 456 not shown because it does not depend on η or δ .
 457
 458

459 For NO₂ the emission decrease (increase) is -76% (+417%).

460 In addition, Fig. 8b shows the emissions depending on the gauge pressure for 1 (lower limit), 5 and
 461 10 psi (upper limit) (7, 34 and 69 kPa respectively) for $\eta = 0.8$ and $\delta = 0.95$. Using 5 psi as the
 462 reference, the lower (upper) limit leads to a decrease (increase) in CO emissions of -20% (+25%).

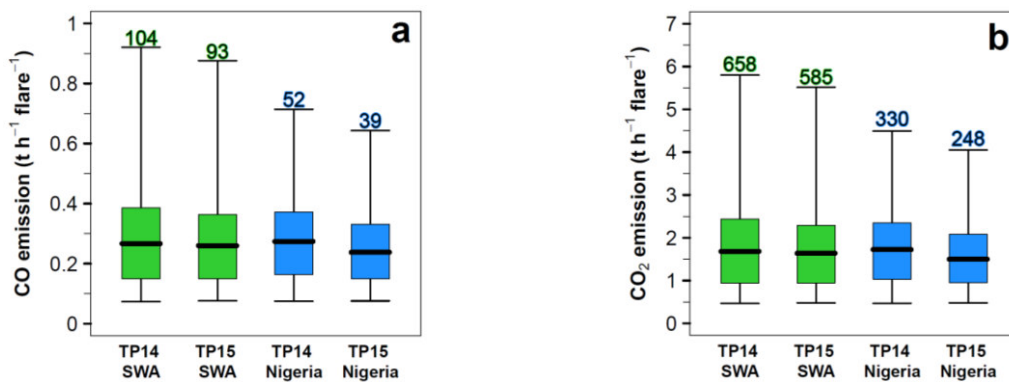
463 Fig. 8 emphasizes that the technical conditions of flaring crucially influence the emission strength and
 464 that the emissions are more sensitive towards η and δ than towards the gauge pressure.
 465

466 3.3.3 Uncertainty due to the fraction of radiated heat

467 To estimate the uncertainty in the fraction of radiated heat f (see Tab. 2), we have used the standard
 468 deviation of the literature values given in the appendix of Guigard et al. (2000) in addition to the
 469 mean value of $f = 0.27$. This leads to a domain of uncertainty for the value f of $(^{0.38}/_{0.16})$. Therefore
 470 the VNF_{flare} observed radiant heat is multiplied with the factor $1/f$ of 3.7 ($^{6.2}/_{2.6}$).
 471

473 3.3.4 Interannual variability

474 The differences in flaring between TP14 and TP15, indicated in Fig. 1 and Fig. 2, are quantified in this
 475 section according to the emissions of CO (Fig. 9a) and CO₂ (Fig. 9b). The boxplots include all flares for
 476 the two domains SWA (green) and Nigeria (blue). The numbers above indicate the integrated
 477 emissions per hour and area in tons.
 478



480 **Fig.9.** Single flaring emissions of (a) CO and (b) CO₂ (E_{clim} , $\text{t h}^{-1} \text{ flare}^{-1}$) for SWA (green) and Nigeria (blue) for TP14 and TP15.
 481 The values above the boxplots indicate the emissions per hour, integrated over SWA (green) and Nigeria (blue). The
 482 whiskers span the data range from the 0.025-quantile to the 0.975-quantile (95% of the data). Data outside of this range is
 483 not shown.
 484

485 The emissions of CO₂ are 6.3 times higher than the CO emissions. For Nigeria (blue boxplots) the
 486 mean value of emissions is statistically significant lower for TP15 compared to TP14 (Wilcoxon-Mann-
 487 Whitney rank sum test with a significance level of 0.05). For SWA the emission averages show no
 488 significant difference. The significant different mean values for Nigeria emphasize the relevance of
 489 using a flaring dataset which is up to date to reduce uncertainties arising from deviations in flare
 490 locations or flaring processes.
 491

493 3.3.5 Uncertainty due to spatial variability in H₂S

494 Since hydrogen sulfide (H₂S) is the only sulfur source in the flared gas, it determines the emission of
 495 sulfur dioxide. The natural gas composition measurements from the ten flow stations given in
 496 Sonibare and Akeredolu (2004) contain only two stations with nonzero H₂S content. Therefore
 497 averaging over the ten stations (see Tab. 3) leads to a low H₂S content in the emission calculations.
 498 By using the highest concentration value of H₂S given in Sonibare and Akeredolu (2004) (see Tab. 3,
 499 H₂S concentration 0.03% instead of 0.005%), we try to estimate the upper limit of SO₂ emission,
 500 assuming that all flares are provided with this more sulfur containing gas. With this approach the
 501

502 temporal averaged sum of SO₂ emissions over SWA increase from 36 to 320 kg h⁻¹. This comparison
 503 reveals that among the flaring conditions also the natural gas composition plays an important role in
 504 estimating the flaring emissions reasonably. To rely on a single measurement dataset for a large
 505 flaring domain and without taking into account spatial variability is therefore problematic but has to
 506 be accepted owing to data shortage.

507 This section has estimated the uncertainties in gas flaring due to cloud cover, parameters of IU14, the
 508 fraction of radiated heat, the temporal variability and the H₂S concentration in the natural gas. The
 509 uncertainty regarding the spatial variability of the total hydrocarbon fraction of the natural gas,
 510 which is estimated by the variations in the ten flow station measurements of Sonibare and Akeredolu
 511 (2004), is below 1%.

512 However, there are further assumptions or sources of uncertainty which cannot be quantified within
 513 this study: We assume that the natural gas composition, which is measured in one region, is valid for
 514 SWA entirely. The gas flares are taken as constant emission sources because VNF_{flare} only provides
 515 one observation (overflight) per day. We cannot take into account the spatial variability of the flares
 516 concerning the IU14 parameters and the stack heights. And finally IU14 delivers no VOCs and black
 517 carbon.

518

519 **4. Comparison with existing emission inventories**

520

521 The following section places the estimated flaring emissions of this study in the context of existing
 522 emission inventories, by taking the focus on CO₂. A direct comparison with existing emission
 523 inventories is problematic due to different reference time periods, spatial domains, definitions of
 524 emission sectors and the limitation of chemical compounds. Tab. 5 summarizes the CO₂ emissions for
 525 different inventories regarding Nigeria as the flaring hotspot of the research domain. To derive
 526 annual emission values for the results of this study, it is assumed that the flaring emission conditions
 527 of TP14 and TP15 are representative for the whole year 2014 and 2015 respectively. Therefore the
 528 hourly emissions are integrated over 365 days. In addition to the three inventories E_{obs}, E_{com} and E_{clim},
 529 whose emissions are derived from temporal averages of the source temperature and radiant heat,
 530 also an emission estimation using instantaneous source temperature and radiant heat (calculating
 531 emissions for every single observation and subsequent temporal averaging of the emissions) for both
 532 time periods is presented in Tab.5 (E_{clim}, instant. input).

533

534 **Tab.5.** Comparison between existing emission inventories for CO₂ (with a focus on gas flaring if available) and the results of
 535 this study for Nigeria in teragram (Tg) per year. For TP14 and TP15 it is assumed that the two month observations represent
 536 the flaring conditions of the whole year 2014 and 2015 respectively. Therefore the emissions were integrated to yearly
 537 values. The domain of uncertainty arising from the UP14 parameters and the spatial variability in total hydrocarbon is given
 538 in brackets. For the fraction of radiated heat *f*, the mean value 0.27 and the lower (upper) boundary of 0.16 (0.38) are
 539 used, representing a further source of uncertainty. The products given in bold are directly related to flaring emissions.

540

Emission inventory	Time period	CO ₂ emissions (Tg y ⁻¹)		
		<i>f</i> = 0.16	<i>f</i> = 0.27	<i>f</i> = 0.38
This study (E_{obs}, averaged)	2014 (from TP14)	1.7 (2.2/0.3)	1.0 (1.3/0.2)	0.7 (1.0/0.1)
This study (E_{com}, averaged)	2014 (from TP14)	4.5 (6.1/0.9)	2.7 (3.6/0.5)	1.9 (2.6/0.3)
This study (E_{clim})	2014 (from TP14)	4.9 (6.5/1.0)	2.9 (3.9/0.6)	2.1 (2.8/0.4)
This study (E_{obs}, averaged)	2015 (from TP15)	1.0 (1.4/0.2)	0.6 (0.8/0.1)	0.4 (0.6/0.0)
This study (E_{com}, averaged)	2015 (from TP15)	3.4 (4.5/0.7)	2.0 (2.7/0.4)	1.4 (2.0/0.3)
This study (E_{clim})	2015 (from TP15)	3.7 (4.9/0.7)	2.2 (2.9/0.4)	1.5 (2.1/0.3)
This study (E_{clim}, instant. input)	2014 (from TP14)	9.9 (13.2/2.0)	5.9 (7.9/1.2)	4.2 (5.6/0.8)

This study (E_{clim}, instant. input)	2015 (from TP15)	8.8 (^{11.8} / _{1.8})	5.2 (^{7.0} / _{1.0})	3.7 (^{4.9} / _{0.7})
CDIAC (2015b)¹	2011		27.47	
EIA (2015)²	2010; 2011; 2013		38.81; 41.39; 52.83	
Doumbia et al. (2014)¹	2010		45	
EDGAR 4.2³ (ECCAD, 2015)	2008		8.75	
EDGAR 4.2⁴ (ECCAD, 2015)	2008		3.50	
EDGAR 4.3.2⁵ (EDGAR, 2016)	2010; 2011; 2012		29.4, 28.8, 28.9	
EDGARv43FT2012⁶ (EDGAR, 2014)	2014		93.87	

541
542
543
544
545
546
547
548
549
550

¹from gas flaring, Nigeria

²from consumption and flaring of natural gas

³from refineries and transformation, Nigeria

⁴from refineries and transformation, Niger Delta area according to Fig. 5a

⁵from venting and flaring of oil and gas production, Nigeria

⁶emission totals of fossil fuel use and industrial processes (cement production, carbonate use of limestone and dolomite, non-energy use of fuels and other combustion). Excluded are: short-cycle biomass burning (such as agricultural waste burning) and large-scale biomass burning (such as forest fires), Nigeria

551 The CO₂ emission estimations of this study are given in Tab. 5 together with an overall uncertainty
552 range of (⁺³³/₋₇₉%) in brackets, including the uncertainty from the IU14 parameters η and δ
553 (⁺¹²/₋₅₃%) and the gauge pressure (⁺²⁰/₋₂₅%) and from spatial variability of total hydrocarbon. The
554 latter uncertainty is small (below 1%) owing to the low variation in THC concentration in the
555 measurements of Sonibare and Akeredolu (2004). The uncertainty owing to the fraction of radiated
556 heat f is represented by using the average value of 0.27 and the upper and lower estimate of 0.16
557 and 0.38 respectively. The uncertainty due to cloud cover is represented by the difference in E_{obs} and
558 E_{com} .

559 By assuming that E_{com} with $f = 0.27$ represents the best emission estimate for this study and by
560 integrating the above mentioned sources of uncertainty, a total Nigerian CO₂ flaring emission of 2.7
561 (^{3.6}/_{0.5}) Tg y⁻¹ for 2014 and 2.0 (^{2.7}/_{0.4}) Tg y⁻¹ for 2015 was derived. Due to the high uncertainties, the
562 two estimates are not statistically different. These values are one order of magnitude smaller than
563 the values from the Carbon Dioxide Information Analysis Center (CDIAC, 2015b), the Energy
564 Information Administration (EIA, 2015) and the EDGARv.4.3.2 (EDGAR, 2016) database. A direct
565 comparison is hindered by a time lag of 3-4 years and missing information about the uncertainties of
566 CDIAC. The values of EIA are higher than those of CDIAC because EIA includes the consumption of
567 natural gas in addition to gas flaring. Doumbia et al. (2014) combines Defense Meteorological
568 Satellite Program (DMSP) observations of flaring with the emission factor method to derive flaring
569 emissions. The results agree with EIA (2015) but are 64% higher than CDIAC (2015b).

570 The emission inventory EDGAR v4.2 (ECCAD, 2015) delivers 8.75 (3.50) Tg CO₂ y⁻¹ for Nigeria (Niger
571 Delta area) for the emission sector *refineries and transformation*, which is in good agreement with
572 the results for the study on hand.

573 As a benchmark for the flaring CO₂, the total CO₂ emissions for Nigeria are given by EDGAR (2014),
574 (fossil fuel use and industrial processes). Taking EDGAR (2014) as a reference for total CO₂ emissions
575 of Nigeria, flaring emissions contribute with 2 (^{3.9}/_{0.0})% (this study for 2014; E_{com}), 9% (2008; ECCAD,
576 2015), 28% (2011; CDIAC, 2015b), 48% (2010; Doumbia et al., 2014) or 56% (2013; EIA, 2015). The
577 large spread between the different inventories emphasizes the large uncertainty within the
578 estimation of emissions from gas flaring.

579 By using the climatological approach with instantaneous source temperature and radiant heat input
580 data (E_{clim} , instant. input) instead of temporal averages (E_{clim}), the emissions are increased by approx.
581 a factor of two (5.9 (^{7.9}/_{1.2}) Tg y⁻¹ for 2014, 5.2 (^{7.0}/_{1.0}) Tg y⁻¹ for 2015). This underlines that also the

582 preprocessing of the remote sensing data for the calculation of the emissions is a considerable
583 source of uncertainty. However, due to the high uncertainties also the two emission estimates with
584 and without instantaneous data are not statistically different.

585 A shortcoming of the PEGASOS_PBL-v2 (not shown) and the EDGAR v4.2 emission inventory is the
586 lack of offshore flaring emissions in the Gulf of Guinea south of Nigeria. For CDIAC and EIA this
587 cannot be verified since the data is only available as a single value per country.

588 The differences between the results of this study and the existing emission inventories might be
589 caused by insufficient information about the efficiency of combustion processes of SWA flares or by
590 an inconsistent definition of emission source sectors for the existing inventories. E_{com} , Doumbia et al.
591 (2014) and CDIAC (2015b) focus on gas flaring, whereas other products also include natural gas
592 consumption and emissions from refineries and transformation, which also can include non-flaring
593 emissions within and outside the areas indicated as flaring area by the satellite imagery. In addition,
594 the existing inventories do not provide current values (time lag of 2 to 6 years) and therefore not
595 consider the emission reduction indicated by Fig. 9.

596

597 **5. Discussion and conclusions**

598

599 The gas flaring emission estimating method of Ismail and Umukoro (2014) (IU14) has been combined
600 with the remote sensing flare location determination of the VIIRS Nightfire Prerun V2.1 Flares only
601 (VNF) (VIIRS, 2015a) for a new flaring emission parameterization. The parameterization combines
602 equations of incomplete combustion with the gas flow rate derived from remote sensing parameters
603 instead of using emission factors and delivers emissions of the chemical compounds CO, CO₂, SO₂, NO
604 and NO₂.

605 Within this study the parameterization was applied to southern West Africa (SWA) including Nigeria
606 as the second biggest flaring country. Two two-month flaring observation datasets for June/July 2014
607 (TP14) and June/July 2015 (TP15) were used to create a flaring climatology for both time periods. In
608 this climatology all detected flares emit with their mean activity (climatological approach).

609 The uncertainties owing to missed flare observations by cloud cover, parameterization parameters,
610 interannual variability and the natural gas compositions were assessed. It can be shown that the
611 highest uncertainties arise from the IU14 parameters ($+^{33}/_{-79}$ %), followed by the definition of the
612 fraction of radiated heat f . The uncertainty arising from flares masked by clouds is estimated as 61%
613 on average in TP15.

614 By using the cloud detection of VNF and by assuming that all cloud-covered flares are active, an
615 additional emission dataset was derived which combines the emissions from the currently observed
616 flares and the climatological emissions from cloud-covered (not detected) flares (combined
617 approach). These emissions are on average 9% smaller than the climatology but 61% larger than the
618 net observations.

619 However, owing to the large uncertainty ranges, no significant difference between the climatological
620 inventory and the combined inventory can be stated. Comparing the emissions of 2014 and 2015, a
621 reduction in the flaring area, density of active flares and a significant reduction in Nigerian flaring
622 emissions about 25% can be observed, which underlines the need for more recent emission
623 inventories.

624 The uncertainty due to the natural gas composition is compound dependent. The spatial variation in
625 total hydrocarbon is negligible but the availability of hydrogen sulfide, which exclusively determines
626 the amount of emitted SO₂, cause large uncertainty. By taking the combustion efficiency to derive
627 the fraction of unburned natural gas, the amount of emitted VOCs might be estimated in addition to

628 the species of the study on hand but would also be linked to high uncertainties concerning the VOC
629 speciation. The uncertainty in VOC emission is increased drastically by natural gas which is vented
630 directly into the atmosphere instead of being flared, since the venting cannot be detected by VNF.
631 With a focus on Nigeria, the CO₂ emission estimates of this study were compared with existing
632 inventories. For the combined approach, CO₂ emissions of 2.7 (^{3.6}/_{0.5}) Tg y⁻¹ for 2014 and 2.0 (^{2.7}/_{0.4})
633 Tg y⁻¹ for 2015 were derived. EDGAR v4.2 for the year 2008 shows the same order of magnitude when
634 limiting to emissions from refineries and transformation. The results of this study are one order of
635 magnitude smaller compared to CDIAC (Carbon Dioxide Information Analysis Center), Doumbia et al.
636 (2014) and EIA (Energy Information Administration). This emission underestimation is not caused by
637 an underestimation of the flared gas volume. VNF_{flare} includes an estimation of the annual sum of
638 flared gas by country. For Nigeria the estimated values are 8.56 (7.64) bcm flared gas in 2014 (2015).
639 Within this study higher values of 37.89 (20.68) bcm for 2014 (2015) are derived.
640 The deviations might be caused by the uncertainty in the efficiency of the flares concerning the
641 combustion process and their operation. A lack of information regarding the combustion efficiency
642 together with the high sensitivity of the parameters within the combustion equations of IU14 can
643 lead to high uncertainties. Additionally, the usage of emission factors in the existing inventories
644 which did not take into account the spatiotemporal variability of flaring, inconsistent emission sector
645 definitions or the time lag of the emission inventories of 2-5 years can cause deviations. The positive
646 trend in Nigerian gas flaring CO₂ emissions derived by EIA from 38.81 to 52.83 Tg y⁻¹ between 2010
647 and 2013 contradicts the findings of Doumbia et al. (2014) and this study, which generally show a
648 decrease in emissions from 1994 to 2010 and from 2014 to 2015, respectively. Based on the
649 sensitivity study, which reveals high uncertainties of the flaring emission, we conclude that there is
650 no preference in the choice of the climatological and or the combined approach presented in this
651 study. Therefore for simplicity we recommend the use of the climatological approach when using the
652 R package.

653 Despite the generally large uncertainties in the estimation of emissions from gas flaring, this method
654 allows a flexible creation of flaring emission datasets for various applications (e.g. as emission
655 inventory for atmospheric models). It combines observations with physical based background
656 concerning the combustion. The use of current data makes it possible to consider present trends in
657 gas flaring. Even the creation of near real-time datasets with a time lag of one day is possible. The
658 emissions are merged on grid predefined by the user and depending on the availability of VNF data,
659 the temporal resolution can be selected from single days to years.

660 An improvement of this parameterization can be achieved by an extension of the IU14 method to
661 black carbon and VOCs and an inclusion of spatial resolved measurements of the natural gas
662 composition in combination with information of the gas flaring processes from the oil producing
663 industry. Gas flaring is just one of the sources of air pollution in SWA and therefore the DACCIIWA
664 field campaign in June-July flaring cannot solely focus on flaring. To provide detailed measurements
665 of the flaring characteristics would go beyond the scope of DACCIIWA. However, within the DACCIIWA
666 aircraft campaign, the EUFAR (European Facility for Airborne Research) mission APSOWA
667 (Atmosphere Pollution from Shipping and Oil platforms in West Africa) was conducted to
668 characterize gaseous and particulate pollutants emitted by shipping and oil and gas extraction
669 platforms off the coast of West Africa. The authors hope that the results of APSOWA bring further
670 insight in the characteristics of gas flaring in SWA.
671
672

673 **Acknowledgments**

674
675 The research leading to these results has received funding from the European Union 7th Framework
676 Programme (FP7/2007-2013) under Grant Agreement no. 603502 (EU project DACCIWA: Dynamics-
677 aerosol-chemistry-cloud interactions in West Africa). We thank Mikhail Zhizhin from Earth
678 Observation Group (EOG) of NOAA for providing us with the extracted flaring information from the
679 VNF product. We are grateful to Godsgift Ezaina Umukoro (Department of Mechanical Engineering,
680 University of Ibadan, Nigeria) for the kind support during the implementation of their combustion
681 reaction theory into our parameterization.

682

683 **Code and/or data availability**

684
685 This publication includes a package of well documented R scripts which is free available for research
686 purposes and enables the reader to create their own gas flaring emission datasets. It includes
687 exemplarily the preprocessing for June/July 2015 with a focus on southern West Africa. You get
688 access to the code via zenodo.org (DOI: 10.5281/zenodo.61151), entitled “Gas flaring emission
689 estimation parameterization v2”.

690

691 **References**

- 692
693 API, 2007: **Pressure-relieving and Depressuring Systems**, ANSI/API STANDARD 521 FIFTH EDITION,
694 JANUARY 2007, ISO 23251 (Identical), Petroleum and natural gas industries – Pressure-relieving and
695 depressuring systems, American Petroleum Institute, Section 7.3.2.4: Design details h), 127
696
697 Bader, A., Baukal, C. E., Bussman, W. Zink, J., 2011: **Selecting the proper flare systems**, American
698 Institute of Chemical Engineers (AIChE), <http://people.clarkson.edu/wwilcox/Design/FlareSel.pdf>,
699 accessed: October 2, 2014
700
701 CDIAC, 2015a: **Global CO₂ Emissions from Fossil-Fuel Burning, Cement Manufacture, and gas**
702 **Flaring: 1751-2008**, Carbon Dioxide Information Analysis Center (CDIAC),
703 http://cdiac.ornl.gov/ftp/ndp030/global.1751_2008.ems, accessed: December 6, 2015
704
705 CDIAC, 2015b: **National CO₂ Emissions from Fossil-Fuel Burning, Cement Manufacture, and gas**
706 **Flaring: 1751-2011**, Carbon Dioxide Information Analysis Center (CDIAC), Fossil-Fuel CO₂ Emissions by
707 Nation, http://cdiac.ornl.gov/ftp/ndp030/nation.1751_2011.ems, accessed: December 3, 2015
708
709 CM SAF, 2015: **Operational Products: CFC – Fractional cloud cover instantaneous data** (MSG disk,
710 CM SAF definition), Version 350;
711 [https://wui.cmsaf.eu/safira/action/viewPeriodEntry?id=11495_14063_15657_15672_16574_19152_](https://wui.cmsaf.eu/safira/action/viewPeriodEntry?id=11495_14063_15657_15672_16574_19152_20532_21207)
712 [20532_21207](https://wui.cmsaf.eu/safira/action/viewPeriodEntry?id=11495_14063_15657_15672_16574_19152_20532_21207), accessed: November 25, 2015
713
714 Doumbia, T., Granier, L., Liousse, C., Granier, C., Rosset, R., Oda, T., Fen Chi, H., 2014: **Analysis of fifty**
715 **year Gas flaring Emissions from oil/gas companies in Africa**, AGU Fall Meeting 2014, Dec 2014, San
716 Francisco, United States. A13E-3217
717
718 Dung, E. J., Bombom, L. S., Agusomu, T. D., 2008: **The effects of gas flaring on crops in the Niger**
719 **Delta, Nigeria**, *GeoJournal*, Vol., 73, 297-305
720
721 Ekpoh, I. J., Obia, A. E., 2010: **The role of gas flaring in the rapid corrosion of zinc roofs in the Niger**
722 **Delta Region of Nigeria**, *Environmentalist*, Vol. 30, 347-352
723

724 ECCAD, 2015: **Emissions of atmospheric compounds & compilation of ancillary data (ECCAD)**,
725 http://eccad.sedoo.fr/eccad_extract_interface/JSF/page_critere.jsf, accessed: December 4, 2015
726
727
728 EDGAR, 2016: **Global Emissions EDGAR v4.3.2**, European Commission, Joint Research Centre
729 (JRC)/PBL Netherlands Environmental Assessment Agency. Emission Database for Global Atmospheric
730 Research (EDGAR), release version 4.3.2. <http://edgar.jrc.ec.europa.eu>
731
732 EDGAR, 2014: **Global Emissions EDGAR v4.3 FT2012**, European Commission, Joint Research Centre
733 (JRC)/PBL Netherlands Environmental Assessment Agency. Emission Database for Global Atmospheric
734 Research (EDGAR), release version 4.3. <http://edgar.jrc.ec.europa.eu>, 2015 forthcoming,
735 <http://edgar.jrc.ec.europa.eu/overview.php?v=CO2ts1990-2014>, accessed: December 3, 2015
736
737 EIA, 2015: **CO₂ from the Consumption and Flaring of Natural Gas**, International Energy Statistics,
738 U.S. Energy Information Administration (EIA),
739 <http://www.eia.gov/cfapps/ipdbproject/iedindex3.cfm?tid=90&pid=3&aid=8&cid=&syid=2010&eyid=2013&unit=MMTCD>, accessed: December 3, 2015
740
741
742 Elvidge, C. D., Zhizhin, M., Baugh, K., Hsu, F.-C., Gosh, T., 2015: Methods for Global Survey of Natural
743 Gas Flaring from Visible Infrared Imaging Radiometer Suite Data, *Energies* 2016, 9, 14, 1-15
744
745 Elvidge, C. D., Zhizhin, M., Hsu, F.-C., Baugh, K. E., 2013: **VIIRS Nightfire: Satellite Pyrometry at Night**,
746 *Remote Sens.*, Vol. 5, 4423-4449
747
748 Elvidge, C. D., Ziskin, D., Baugh, K. E., Tuttle, B. T., Gosh, T., Pack, D. W., Erwin, E. H., Zhizhin, M.,
749 2009: **A fifteen year record of global natural gas flaring derived from satellite data**, *Energies*, Vol. 2,
750 595-622
751
752 Elvidge, C. D., Baugh K. E., Kihn, E. A., Kroehl, H. W., Davis, E. R., 1997: **Mapping city lights with
753 nighttime data from the DMSP operation linescan system**, *Photogrammetric Engineering & Remote
754 Sensing*, Vol. 63, No. 6, 727-744
755
756 EPA, 1985: **Evaluation of the efficiency of industrial flares: Flare head design and gas composition**,
757 Research and Development, United States Environmental Protection Agency (EPA), EPA-600/2-85-
758 106, Tab. 2-6
759
760 Google Earth, 2014: Image 2014 DigitalGlobe, <http://www.earth.google.com>
761
762 Guigard, S. E., Kindzierski, W. B., Harper, N., 2000: **Heat Radiation from Flares**. Report prepared for
763 Science and Technology Branch, Alberta Environment, ISBN 0-7785-1188-X, Edmonton, Alberta.
764
765 Ismail, O. S., Umukoro, G. E., 2014: **Modelling combustion reactions for gas flaring and its resulting
766 emissions**, *Journal of King Saud University – Engineering Sciences*, Vol. 28, 130-140
767
768 Johnson, M. R., Devillers, R. W., Thomson, K. A., 2011: **Quantitative Field Measurements of Soot
769 Emission from Large Gas Flare using Sky-LOSA**, *Environ. Sci. Technol.*, Vol. 45, 345-350
770
771 Knippertz, P., Evans, M. J., Field, P. R., Fink, A. H., Liousse, C., Marsham, J. H., 2015: **The possible role
772 of local air pollution in climate change in West Africa**, *Nature Climate Change*, Vol. 5, 815-822
773
774 Mirador, 2016: AIRS/Aqua Level 2 Standard physical retrieval (AIRS+AMSU), Total cloud fraction
775 (CldFrcTot), [mirador.gsfc.nasa.gov/cgi/bin/mirador/presentNavigation.pl?tree=project&
776 Project=AIRS&data](http://mirador.gsfc.nasa.gov/cgi/bin/mirador/presentNavigation.pl?tree=project&Project=AIRS&data), accessed: April 18, 2016
777
778 NASA, 2016: <http://npp.gsfc.nasa.gov/viirs.html>, accessed: January 5, 2016

779
780 Nwankwo, C. N., Ogagarue, D., O., 2011: **Effects of gas flaring on surface and ground waters in Delta**
781 **State Nigeria**, Journal of Geology and Mining Research, Vol. 3, 131-136
782
783 Nwaugo, V. O., Onyeagba, R. A., Nwahcukwu, N. C., 2006: **Effect of gas flaring on soil microbial**
784 **spectrum in parts of Niger Delta area of southern Nigeria**, African Journal of Biotechnology, Vol. 5,
785 1824-1826
786
787 Osuji, L. C., Avwiri, G. O., 2005: **Flared Gas and Other Pollutants Associated with Air quality in**
788 **industrial Areas of Nigeria: An Overview**, Chemistry & Biodiversity, Vol. 2, 1277-1289
789
790 R Core Team, 2013: **R: A Language and Environment for Statistical Computing**, R Foundation for
791 Statistical Computing, Vienna, Austria, <http://www.R-project.org/>
792
793 Sonibare, J. A., Akeredolu, F. A., 2004: **A theoretical prediction of non-methane gaseous emissions**
794 **from natural gas combustion**, Energy Policy, Vol. 32, 1653-1665
795
796 Strosher, M. T., 2000: **Characterization of Emissions from Diffuse Flare Systems**, Journal of the Air &
797 Waste Management Association, 50:10, 1723-1733
798
799 Strosher, M. T., 1996; **Investigations of flare gas emissions in Alberta**, Final Report to: Environment
800 Canada, Conservation and protection, the Alberta Energy and Utilities Board, and the Canadian
801 Association of Petroleum Producers; Environmental Technologies, Alberta Research Council, Calgary,
802 Alberta
803
804 van der Linden, R., Fink, A. H., Redl, R., 2015: **Satellite-based climatology of low-level continental**
805 **clouds in southern West Africa during the summer monsoon season**, Journal of Geophysical
806 Research: Atmospheres, Vol. 120, 1186-1201
807
808 VDI 3782, 1985: Dispersion of Air Pollutants in the Atmosphere, Determination of Plume rise, Verein
809 Deutscher Ingenieure, VDI-Richtlinien 3782 Part 3, Equation 24, [https://www.vdi.de/richtlinie/
810 vdi_3782_blat_3-ausbreitung_von_luftverunreinigungen_in_der_atmosphaere_berechnung_der_
811 abgasfahnenueberhoehung/](https://www.vdi.de/richtlinie/vdi_3782_blat_3-ausbreitung_von_luftverunreinigungen_in_der_atmosphaere_berechnung_der_abgasfahnenueberhoehung/), accessed: October 17, 2016
812
813 VIIRS, 2015a: http://ngdc.noaa.gov/eog/viirs/download_viirs_fire.html, accessed: August 24, 2016
814
815 VIIRS, 2015b: http://ngdc.noaa.gov/eog/viirs/download_viirs_flares_only.html, accessed: July 31,
816 2015
817
818 Vogel, B., Vogel, H., Bäumer, D., Bangert, M., Lundgren, K., Rinke, R., Stanelle, T., 2009: **The**
819 **comprehensive model system COSMO-ART - Radiative impact of aerosol on the state of the**
820 **atmosphere on the regional scale**, Atmos. Chem. Phys., 9, 8661-8680
821
822 World Bank, 2012: [http://www.worldbank.org/content/dam/Worldbank/Programs/Top_20_gas
823 flaring_countries.pdf](http://www.worldbank.org/content/dam/Worldbank/Programs/Top_20_gas_flaring_countries.pdf), accessed: December 5, 2015
824
825 Zhang, X., Scheving, B., Shoghli, B., Zygarlicke, C., Wocken, C., 2015: **Quantifying Gas Flaring CH₄**
826 **Consumption Using VIIRS**, Remote Sens., Vol. 7, 9529-9541
827